Impact of biexcitons on the relaxation mechanisms of polaritons in III-nitride based multi-quantum well microcavities.

P. Corfdir, J. Levrat, G. Rossbach, R. Butté, E. Feltin, J.F. Carlin, G. Christmann, Pierre Lefebvre, Jean-Daniel Ganière, N. Grandjean, et al.

Impact of biexcitons on the relaxation mechanisms of polaritons in III-nitride based multiple quantum well microcavities

P. Corfdir,[1,2,*] J. Levrat,[1] G. Rossbach,[1] R. Butté,[1] E. Feltin,[1] J.-F. Carlin,[1] G. Christmann,[1,†] P. Lefebvre,[3,4] J.-D. Ganière,[1] N. Grandjean,[1] and B. Deveaud-Plédran[1]

[1]*Institute of Condensed Matter Physics, Ecole Polytechnique Fédérale de Lausanne (EPFL), 1015 Lausanne, Switzerland*

[2]*Cavendish Laboratory, University of Cambridge, J. J. Thomson Avenue, Cambridge CB3 0HE, United Kingdom*

[3]*CNRS, Laboratoire Charles Coulomb, UMR5221, F-34095 Montpellier, France*

[4]*Université Montpellier 2, Laboratoire Charles Coulomb, UMR5221, F-34095 Montpellier, France*

(Received 8 February 2012; revised manuscript received 3 April 2012; published 13 June 2012)

We report on the direct observation of biexcitons in a III-nitride based multiple quantum well microcavity operating in the strong light-matter coupling regime by means of nonresonant continuous wave and time-resolved photoluminescence at low temperature. First, the biexciton dynamics is investigated for the bare active medium (multiple quantum wells alone) evidencing localization on potential fluctuations due to alloy disorder and thermalization between both localized and free excitonic and biexcitonic populations. Then, the role of biexcitons is considered for the full microcavity: in particular, we observe that for specific detunings the bottom of the lower polariton branch is directly fed by the radiative dissociation of either cavity biexcitons or excitons mediated by one LO-phonon. Accordingly, minimum polariton lasing thresholds are observed, when the bottom of the lower polariton branch corresponds in energy to the exciton or cavity biexciton first LO-phonon replica. This singular observation highlights the role of excitonic molecules in the polariton condensate formation process as being a more efficient relaxation channel when compared to the usually assumed acoustical phonon emission one.

DOI: 10.1103/PhysRevB.85.245308 PACS number(s): 78.67.De, 78.47.jd

I. INTRODUCTION

In planar semiconductor microcavities (MCs), the strong coupling between excitons and photons gives rise to admixed quasiparticles called exciton polaritons.[1] Thanks to the unique properties coming from their dual light and matter nature, they raise great interest in the scientific community. We mention, for instance, parametric amplification,[2] massive occupation of the polariton ground state through Bose-Einstein condensation[3] or polariton lasing.[4] As a consequence, MC polaritons offer the possibility of achieving coherent light emission with a threshold lower than that of conventional semiconductor lasers[5] as it is not ruled by the Bernard-Duraffourg condition. The main limitation to achieve polariton lasing is the efficiency of the polariton relaxation from the excitonic reservoir to the bottom of the lower polariton (LP) branch (LPB).[6] To realize such a condensate under nonresonant excitation, the relaxation rate of polaritons from the exciton reservoir to the center of the Brillouin zone must indeed exceed their radiative decay.[7,8] However, due to their strong photonic character, LPs with a zero in-plane wave vector $\mathbf{k}_{\parallel} = 0$ exhibit a radiative lifetime of the order of 0.1 to 10 ps, and it is therefore mandatory to inject a sufficiently high density of carriers to reach the stimulated scattering regime. In parallel, increasing the polariton density may lead to exciton screening and phase-space filling. Consequently, in GaAs MCs, the strong coupling regime (SCR) might be lost before reaching the nonlinear regime,[9] and great care must be taken when designing the MC sample so as to increase either the polariton lifetime,[10] the stability of polaritons,[11] or the interaction strength.[12,13]

On the contrary, the large exciton binding energy in GaN-based heterostructures shifts the Mott transition to much higher critical temperatures ($T_{\mathrm{crit}} \sim 540$ K)[14] and critical carrier densities [$n_{\mathrm{crit}} \sim 10^{12}$ cm^{-2} per quantum well (QW),[15]] allowing for the buildup of a polariton condensate at room temperature both in bulk[4] and multiple quantum well (MQW) nitride-based planar MCs.[16] It was shown experimentally[17] that the polariton lasing threshold critically depends on the temperature and the detuning $\delta = E_c(0) - E_X(0)$, with $E_X(0)$ and $E_c(0)$ the energy of the QW exciton and cavity photon at $\mathbf{k}_{\parallel} = 0$, respectively. Although such a behavior can be qualitatively described by accounting for the temperature- and δ-dependences of the scattering rates by solving numerically semiclassical Boltzmann equations,[14] the system is definitely more complex. We mention, in particular, the role played by disorder,[18,19] dark exciton states, and biexcitons.[20] The latter have indeed been shown to be instrumental in analyzing four-wave mixing experiments performed on GaAs MCs.[21–23] The SCR between the biexciton transition and the cavity photon might even be observed in MCs submitted to intense circularly polarized excitation.[24] Compared to III-As or II-VI MQW MCs, disorder and biexcitons should play an even more important role in nitride-based systems. First, GaN MCs exhibit a significant disorder.[25] One, thus, expects a significant part of the oscillator strength from the LPs and the upper polaritons (UPs) to be shared with the uncoupled "dark" exciton modes in MQW MCs.[26] In addition, excitons confined in GaN QWs efficiently bind into biexcitons.[27] In bulk GaN, the biexciton binding energy is of the order of 5.7 meV.[28,29] In systems of reduced dimensionality, the biexciton binding energy varies in a non-trivial way as it depends on the confinement, the disorder, and the amplitude of the quantum-confined Stark effect inherent to III-nitride based heterostructures grown along the polar c axis.[30] In any case, in high-quality nitride-based MQW MCs, where the biexciton binding energy exceeds the exciton inhomogeneous broadening, it should be possible to observe additional emission features linked to the existence of biexcitons.[20] Alternatively, the formation of biexcitons could also play a

major role on the polariton laser threshold, as the LPB may be directly fed by the radiative dissociation of biexcitons.[20]

Here, we address the role played by biexcitons on the overall relaxation mechanisms in III-nitride MQW MCs by a combined reflectivity and photoluminescence (PL) study. We first observe biexciton emission from the bare-MQW active medium. In particular, we extract both biexciton binding and localization energies, and we describe the localization dynamics of biexcitons along the QW planes. We then turn our attention to the full-MC sample. Because of the disorder specific to III-nitride MC samples, polaritons partly share their oscillator strength with dark excitons, making it possible to observe these latter states via reflectivity and PL experiments. Next, we evidence that dark excitons efficiently bind into cavity biexcitons, which radiatively dissociate leaving an LP in the reservoir or a dark exciton. In the linear regime, when the energy of the first LO-phonon replica of the cavity biexciton matches that of the bottom of the LPB, an increase in the LP emission intensity at $\mathbf{k}_{\parallel} = 0$ is observed. In addition, we observe for this detuning a minimum polariton lasing threshold. Consequently, in this specific detuning case, the relaxation of LPs toward the center of the Brillouin zone is limited by the radiative dissociation of cavity biexcitons rather than by the scattering of higher-$\mathbf{k}_{\parallel}$ LPs by acoustic phonons.

The paper is organized as follows. In Sec. II, we present the structure of the investigated samples and describe the experimental setups. In Sec. III, we identify the emission from biexcitons confined along the QW planes. We then describe how to obtain the biexciton binding and localization energies, an accurate determination of these two energies being mandatory to understand the role played by biexcitons in the full-MC sample. The emission properties of the MC sample are depicted in Sec. IV A, while the emission from cavity biexcitons is identified in Sec. IV B. The role played by biexcitons in the relaxation dynamics of LPs is discussed in Sec. IV C, and we draw our conclusions in Sec. V.

II. EXPERIMENTAL DETAILS

We consider here separately a GaN-based MQW 3λ-MC and its bare active medium, which consists of a 67-period GaN (1.2 nm)/$Al_{0.2}Ga_{0.8}N$ (3.6 nm) stack. Both samples have been grown by metal organic vapor phase epitaxy (MOVPE)[31] on a 3 μm thick GaN buffer deposited on a *c*-plane sapphire substrate. The first sample investigated here, i.e., the bare-MQW sample, was capped by a λ/4 thick $Al_{0.2}Ga_{0.8}N$ layer. The structure of the full MC, already described elsewhere (see Fig. 1 in Ref. 15 for a cross-section transmission electron micrograph of the sample), consists of a high-reflectivity epitaxial 35-pair lattice-matched $Al_{0.85}In_{0.15}N/Al_{0.2}Ga_{0.8}N$ distributed Bragg reflector (DBR) grown on a strain relieving template made of two GaN/AlN superlattices separated by a GaN interlayer followed by an $Al_{0.2}Ga_{0.8}N$ layer. We then grew on top of the bottom DBR the 3λ active medium, consisting of the 67 QWs sandwiched between two λ/4 $Al_{0.2}Ga_{0.8}N$ layers. We finally deposited a 67 nm-thick Si_3N_4 layer and a 13 pair top dielectric SiO_2/Si_3N_4 DBR. As previously shown in Refs. 15 and 16, the entire structure is crack-free. We emphasize that in this specific MC sample, polariton lasing has been reported over the whole 4 to 340 K temperature range for cavity detunings comprised between 0 and −120 meV under quasi-continuous-wave (cw) excitation as detailed in Refs. 14 and 17. Contrary to other MQW-based MC structures operating in the SCR, the present QWs are not located at the antinodes of the electromagnetic standing wave but homogeneously distributed over the full active region. This particular design has been chosen to remove from the QW emission any source of inhomogeneous broadening induced by the variation of the built-in electric field from one QW to the other.[32] We point out that both bare-MQW and full-MC samples have been grown during the same run. Consequently, it is likely that they exhibit similar barrier alloy disorder. We emphasize that the strain state of the GaN layers that constitute the QWs should, however, be different in the two samples, given the very different underlying layer morphology. More specifically, compared to the bare-MQW sample, the QWs in the MC sample are more compressively strained, and therefore their excitonic emission line will appear at higher energy (by ∼60 meV).

We notice that, although the present samples have been grown along the polar [0001] axis, we will hereafter neglect the effect of the built-in electric field on the relaxation and recombination mechanisms of excitons. Indeed these GaN QWs are thin enough to ensure an optimal overlap between electron and hole wave functions even in the presence of the electric field. To check this assumption, we have performed envelope function calculations in the effective potential formalism.[33–35] (Fig. 1). We have included a variational modeling of the exciton, in which we separate the in-plane and on-axis motions of the electron-hole pair.[36] We find that the dynamical descreening of the built-in electric field after pulsed photo-excitation[37] should affect neither the exciton binding energy ($E_X^B = 43$ meV) nor the square modulus of the overlap integral between electron and hole wave functions ($|\langle\Psi_e|\Psi_h\rangle|^2 = 0.9$), and therefore we expect no time- or excitation-dependent change of the exciton radiative lifetime.

Continuous-wave and quasi continuous-wave micro-PL studies were carried out using either a frequency-doubled Ar-ion laser (λ = 244 nm) or a pulsed frequency-quadrupled Nd:YAG laser (λ = 266 nm) with a repetition rate of 8.52 kHz and 500 ps pulse width. For the micro-PL experiments a UV microscope objective with a numerical aperture of 0.55 was used, and the laser beam was focused down to a spot diameter not larger than 2 μm. The collected signal was sent to a 55 cm focal length monochromator followed by a liquid-nitrogen cooled UV-enhanced charge-coupled device. We estimate the spectral resolution of our system to be ∼100 μeV. To image the eigenmode dispersion of the full MC, the back focal plane of the microscope objective (Fourier-plane) was imaged on the entrance slit of the spectrometer via two lenses with focal lengths of 30 and 20 cm, respectively. We also performed in the same configuration microreflectivity measurements with a 150 W Xe lamp (note that the experiments displayed in Fig. 5 have been taken with a two-arm goniometer in θ-θ configuration, the incoming light beam being brought by a 100 μm core fiber, while the reflected light was then collected by a 400 μm core fiber; the overall setup offering an angular selection of 1°). PL excitation (PLE) measurements were performed with an optical parametric oscillator- (OPO-) based laser system with an emission wavelength continuously tunable between 200 nm and 2.3 μm pumped by a pulsed Nd:YAG laser

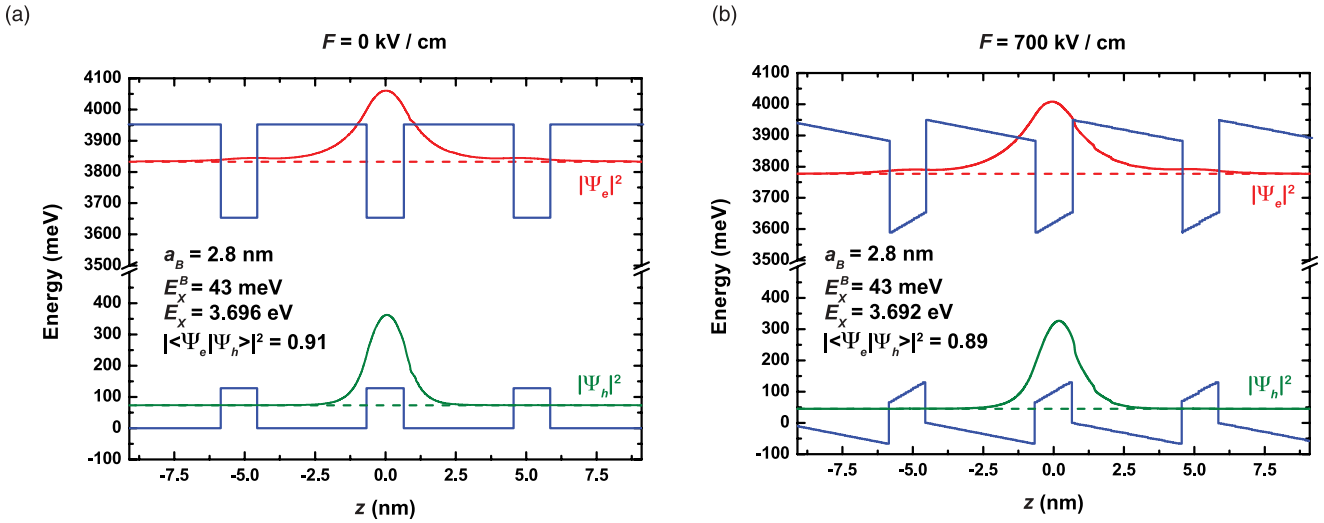

FIG. 1. (Color online) Band profiles (blue line) and electron and hole square modulus of the envelope functions [red (dark gray) and green (medium gray) curves, respectively] for an exciton confined in GaN (1.2 nm)/$Al_{0.2}Ga_{0.8}N$ (3.6 nm) MQW without (a) and with built-in electric field (b). Dotted lines show the confined energy levels. We considered in (b) a 700 kV/cm built-in electric field, which is comparable to what has been observed in similar structures (Ref. 48). a_B, E_X, and E_X^B are the exciton in-plane Bohr radius, transition energy, and binding energy, respectively, while $|\langle\Psi_e \mid \Psi_h\rangle|^2$ is the square modulus of the overlap integral between electron and hole wave functions.

($\lambda = 355$ nm with a 1 kHz repetition rate and 3 ns pulse width). Continuous-wave PL, reflectivity, and PLE experiments were all carried out using a continuous-flow liquid-helium cryostat, which allowed tuning the temperature from 4 to 300 K. For all these experiments (PL, reflectivity, and PLE), we estimate the spot diameter to be of the order of 4 to 5 μm. Time-integrated (TI) and time-resolved (TR) PL experiments were carried out with the third harmonic of a Ti:Al_2O_3 mode-locked laser (pulse width and repetition rate of 2 ps and 80.7 MHz, respectively). For all TI and TR PL experiments, the energy per excitation pulse was kept below 2 pJ. We tuned the excitation wavelength to 280 nm in order to fall into a reflectivity minimum of the Bragg reflector. The laser beam was focused down to a 50 μm-diameter spot on the sample surface. The PL was analyzed with a 1200 grooves/mm grating (spectral resolution of $\sim$500 μeV) followed by an Optronis streak camera working in synchroscan mode.

III. OPTICAL CHARACTERIZATION OF THE MQW SAMPLE

In this section, we identify the emission from biexcitons confined along the QW planes. We then extract both the biexciton binding and localization energies from PL, PLE, and reflectivity experiments and finally characterize by TR PL the impact of interface roughness on the biexciton localization dynamics. The observation of biexciton emission from the MQW sample is demonstrated in Fig. 2. At 4 K, two transitions lying at 3.655 and 3.639 eV dominate the spectrum [Fig. 2(a)]. Under cw conditions, increasing the excitation density leads to a superlinear increase in the intensity of the lower-energy transition with respect to the emission at 3.655 eV [Fig. 2(a)]. Similarly to what was reported in Refs. 30 and 38, the power dependence of the emissions at 3.655 and 3.639 eV allows us to attribute them to the emission from the fundamental QW exciton state (exciton A) and from biexcitons (XX), respectively. Importantly, at low temperatures, the QW emission properties are dominated by localized exciton ($X_{\rm loc}$) states,[39] and the exciton emission energy Δ_X is given by:

$$\Delta_X = E_X - E_X^{\rm loc}, \tag{1}$$

where E_X is the energy of free excitons (FXs) with an in-plane wave vector $\mathbf{k}_\parallel = 0$ and $E_X^{\rm loc}$ is the exciton localization energy. In GaN QWs, potential fluctuations arise from single or bilayer well width variations[40] as well as from barrier alloy disorder.[31] While PLE and reflectivity measurements give access to the energy of the (delocalized) excitonic resonances X_A and X_B, we observe by PL experiments the emission from $X_{\rm loc}$ [Fig. 2(b)]. From the energy difference between X_A and $X_{\rm loc}$, we deduce $E_X^{\rm loc} = 11$ meV [Fig. 2(b)]. This energy seems quite small compared to the 40 meV that we calculate by envelope function calculations for the localization energy of an exciton on a single-monolayer well-width fluctuation. As a matter of fact, it has already been shown that in MOVPE-grown (Al,Ga)N/GaN QWs, Al-content fluctuations in the (Al,GaN) barriers play the most important role in the QW emission inhomogeneous linewidth.[31] From the S-shaped temperature-dependence of the (Al,Ga)N emission energy [Fig. 2(c)], we extract an exciton localization energy of 30 meV in the disordered alloy.[41] We, therefore, account for these fluctuations in the (Al,Ga)N energy band gap in our calculations, and we find that they induce a QW exciton localization energy of approximately 12 meV. In addition to the emission from the (Al,Ga)N barriers and from X and XX confined along the QW planes, we observe at 3.564, and 3.548 eV the emission from the X and XX first LO-phonon replica, respectively, as well as the emission from the GaN buffer layer: the donor-bound A-exciton centered at 3.481 eV and the FX lines A and B at 3.488 and 3.497 eV, respectively [Fig. 2(b)]. Finally, although we observe by reflectivity and PLE a clear resonance from the B QW exciton [Fig. 2(b)], we will hereafter neglect its role on the relaxation and recombination processes

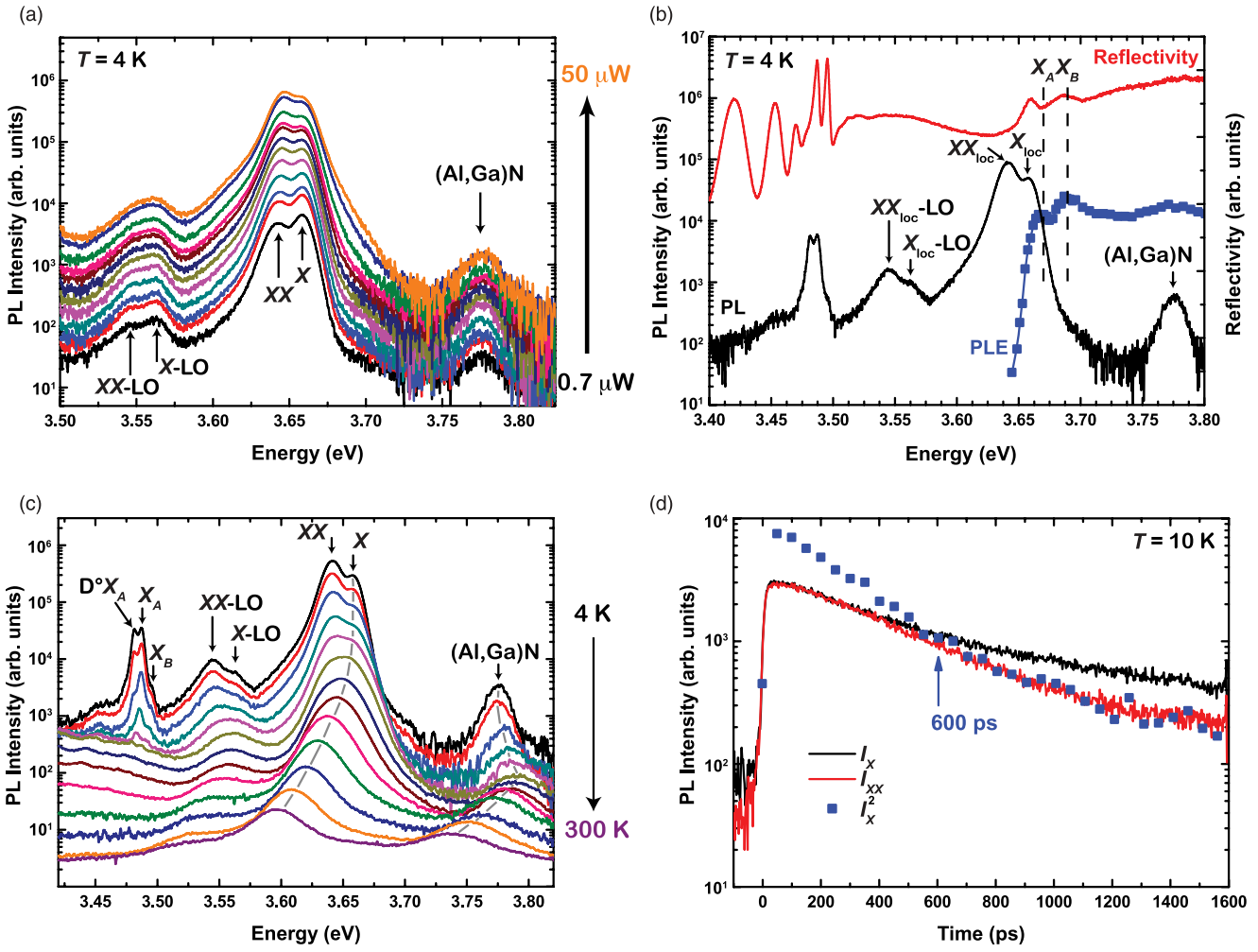

FIG. 2. (Color online) (a) Power-dependent PL spectra of the $Al_{0.2}Ga_{0.8}N$/GaN MQW sample measured at 4 K taken under quasi-cw conditions. The line at 3.639 eV shows a superlinear increase with excitation power with respect to that of the exciton (X), evidencing its biexcitonic origin. (b) Continuous-wave PL (black), reflectivity [red (dark gray)] and PLE [blue (medium gray)] spectra measured at 4 K. The energies of X_A and X_B are deduced from the deconvolution of the PLE spectrum. For the PLE spectrum, the wavelength of the excitation laser was scanned with a 0.2 nm step width. We deduce from the energy difference between PLE and PL spectra a localization energy of 11 meV for excitons confined in the MQWs. (c) Continuous-wave PL spectra for the $Al_{0.2}Ga_{0.8}N$/GaN MQWs from 4 to 300 K. Spectra have been shifted vertically for clarity. Increasing the temperature leads to a quenching of the biexciton emission. In (b) and (c), cw PL spectra have been taken with a frequency-doubled Ar^+ laser ($\lambda = 244$ nm) with an excitation power density of 175 W/cm^2. Note also that in (b) and (c), the lines below 3.51 eV arise from the 3 μm thick GaN buffer. (d) Low-temperature PL time decays for the exciton (black) and biexciton [red (dark gray)] emissions. After 600 ps, the biexciton emission intensity follows the same time dependence as the square of the exciton emission intensity (blue symbols), evidencing full thermalization between exciton and biexciton states. Note that the biexciton PL decay has been spectrally integrated over the emission from free and localized biexcitons.

of carriers. We indeed measure an energy difference of 21 meV between A and B QW excitons. Therefore, for a lattice temperature of 10 K, this higher-energy exciton branch should not be thermally populated.

The biexcitonic origin of the 3.639 eV line is fully consistent with TR-PL data [Fig. 2(d)]. Indeed, at quasithermal equilibrium, exciton and biexciton emission intensities (I_X and I_{XX}, respectively) verify at all times $I_X(t)^2 \propto I_{XX}(t)$[38] (see Appendix, where the validity of this expression is also shown between localized excitons and localized biexcitons). Experimentally, we observe that it takes ~600 ps for the mass action law between excitons and biexcitons to be satisfied. Such a long delay between biexciton formation and the realization of thermal equilibrium between exciton and biexciton densities was previously attributed to the partial decoupling of exciton and biexciton dynamics, once these carriers are localized.[27] Although the detailed discussion of the thermalization dynamics between excitons and biexcitons is outside the scope of this paper, we also presume that the thermalization time between excitons and biexcitons is related to the quantum-confined Stark effect and thus mainly depends on the thickness of the QW.

As it is the case for excitons, biexcitons are bound to potential fluctuations at low temperatures.[42,43] We, thus, define the biexciton localization energy E_{XX}^{loc} as the energy difference between biexcitons free to move along the QW plane and biexcitons bound to potential fluctuations [Fig. 3(a)], giving

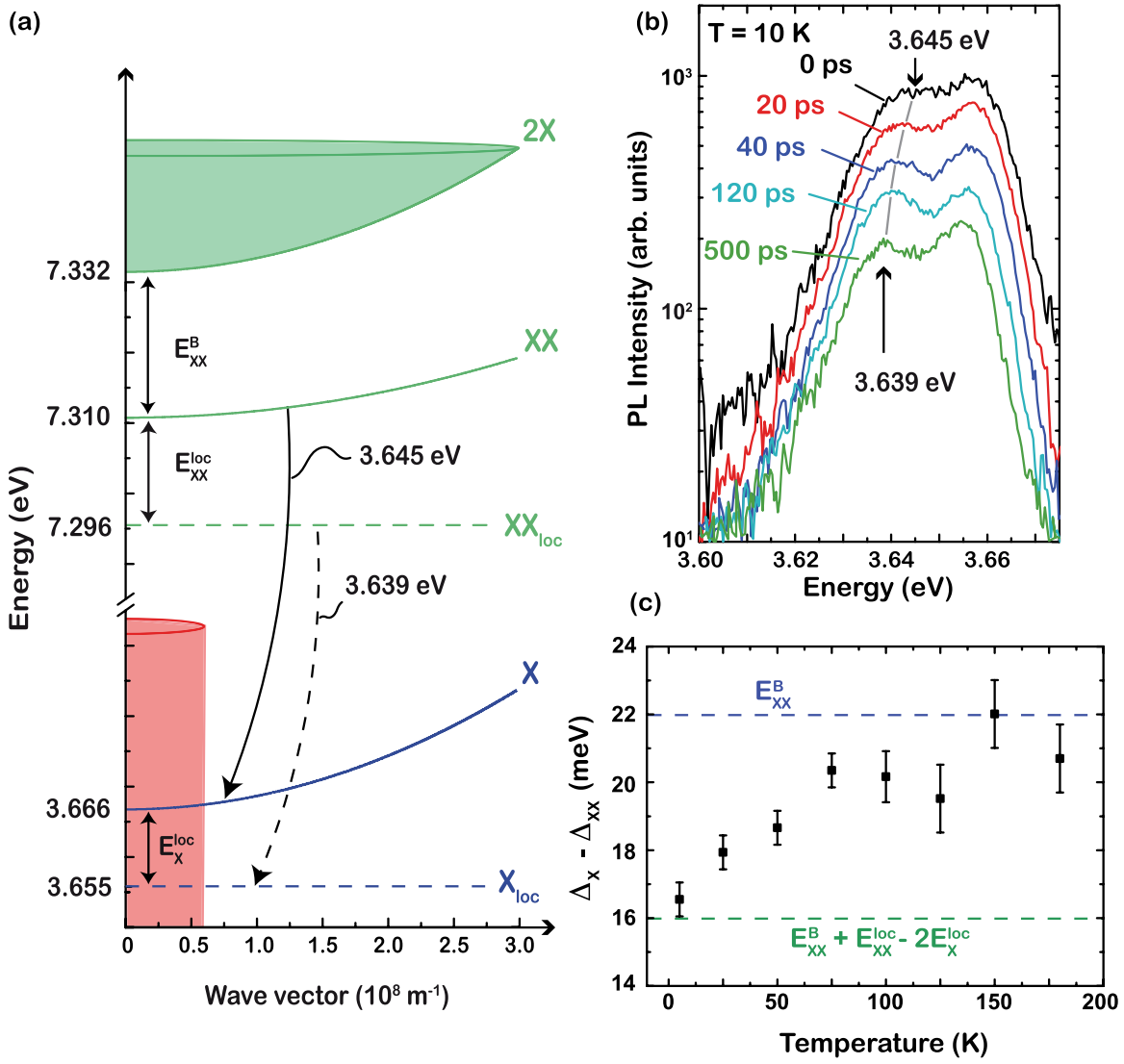

FIG. 3. (Color online) (a) In-plane dispersion of excitons (X) and biexcitons (XX) confined in an $Al_{0.2}Ga_{0.8}N$/GaN QW. Due to the conservation of the in-plane momentum, only excitons lying within the light cone (red) can couple to the light. Biexcitons form from the binding of two excitons ($2X$). The energy difference between the bottom of the two-exciton continuum and a biexciton with zero-kinetic energy is equal to the biexciton binding energy E^B_{XX}. At 10 K, excitons and biexcitons are localized along the QW plane, with respective localization energy $E^{\rm loc}_X$ and $E^{\rm loc}_{XX}$. (b) Time evolution of the MQW PL after nonresonant excitation. At zero delay, the biexciton emission is centered at 3.645 eV. It then redshifts and reaches 3.639 eV after 500 ps. For longer delays, the biexciton emission energy remains constant. This redshift provides a direct observation of the trapping of free biexcitons by potential fluctuations. (c) Temperature dependence of the energy difference between exciton and biexciton PL lines. At 10 K, excitons and biexcitons are localized, and their emission energy difference is given by $\Delta_X - \Delta_{XX} = E^B_{XX} + E^{\rm loc}_{XX} - 2E^{\rm loc}_X = 16$ meV. When the temperature is increased, the energy difference between exciton and biexciton emissions evolves, due to their delocalization along the QW plane. At 200 K, excitons and biexcitons are fully delocalized, and we extract $\Delta_X - \Delta_{XX} = E^B_{XX} = 22$ meV.

for the biexciton emission energy Δ_{XX}:

$$\begin{aligned}\Delta_{XX} &= \left(2E_X - E^B_{XX} - E^{\rm loc}_{XX}\right) - \left(E_X - E^{\rm loc}_X\right)\\ &= E_X + E^{\rm loc}_X - E^{\rm loc}_{XX} - E^B_{XX},\end{aligned} \tag{2}$$

where E^B_{XX} is the biexciton binding energy. Since the recombination of a localized biexciton leaves an exciton that is localized on the same site,[44] the energy difference *at low temperature* between exciton and biexciton emissions is given by:

$$\Delta_X - \Delta_{XX} = E^B_{XX} + E^{\rm loc}_{XX} - 2E^{\rm loc}_X. \tag{3}$$

With increasing temperature, excitons and biexcitons get delocalized over the whole QW plane, and one gets back to the usual relation for the difference between exciton and biexciton emission energies:

$$\Delta_X - \Delta_{XX} = E^B_{XX}. \tag{4}$$

Experimentally, we observe that the energy difference between exciton and biexciton emissions goes from 16 meV at 10 K to 22 meV at 200 K [Fig. 3(c)]. Assuming that excitons and biexcitons are delocalized at 200 K, we deduce $E^B_{XX} = 22$ meV and $E^{\rm loc}_{XX} = 16$ meV (we verify *a posteriori*

that these binding and localization energies are consistent with exciton and biexciton populations that are mostly delocalized at 200 K—see Appendix). Since we estimate by envelope function calculations the exciton binding energy to be 43 meV (Fig. 1), we get $E^B_{XX}/E^B_X = 0.51$. Consequently, not only in bulk ternary alloy[42] but also in QWs, disorder leads to a deviation from the Haynes rule for the binding energy of the biexciton.[45] In addition, from the biexciton binding and localization energies determined above, we deduce that, at 10 K, free and localized QW biexciton emissions should lie at 3.645 and 3.639 eV, respectively. Figure 3(b) shows the low-temperature time evolution of QW exciton and biexciton PL after nonresonant excitation. Just after the excitation, the biexciton emission is centered, indeed, at 3.645 eV. It then redshifts, reaching 3.639 eV after 500 ps, and then its position remains constant for longer delays. Similarly to what was observed for excitons confined in GaAs QWs with single-monolayer well-width fluctuations,[46] this dynamical redshift provides a direct observation of the trapping of free biexcitons by potential fluctuations along the QW plane.

IV. OPTICAL CHARACTERIZATION OF THE MQW MC SAMPLE

A. Emission properties of excitons in the MQW MC

We now turn our attention to the relaxation dynamics of exciton polaritons in the MQW MC sample. The MC structure features a cavity mode with a quality factor $Q \sim 1000$[15] coupled with $N = 67$ independent QW excitons. In *ideal* samples, i.e., in absence of disorder and for fully coupled QWs, the system, operating in the SCR, is described by $N + 1$ eigenstates: two bright modes, the LPs and UPs, and $N - 1$ exciton modes not coupled to the light, the dark excitons.[20] We wish to emphasize that those dark excitons are not dark from spin arguments, but only result from the diagonalization of the Hamiltonian describing the interaction between a cavity mode with N exciton states. Although necessarily present, we will disregard, from now on, the role played by excitons with a total angular momentum $J = 2$, as well as that of biexcitons made out of $J = 2$ excitons, in the overall relaxation scheme.[48]

The interest in working with such MQW MC arises naturally from the fact that

(i) the exciton binding energy in (narrow polar) QWs is increased compared to the bulk case[36,47] by a factor roughly equal to 2,

(ii) the vacuum Rabi splitting scales with the square root of the effective number N_{eff} of QWs inserted in the cavity.[49] Note, however, that due to the homogeneous distribution of QW over the full active region in our sample, $N_{\text{eff}} \sim 33.5$. This means that half of the QWs do not participate in the strong light-matter interaction with the external vacuum field and act as a source of losses for the system,

(iii) the threshold power density is expected to be decreased by a factor of 10 compared to the bulk case due to modified matrix elements for the exciton-exciton interaction,[50] while the exciton saturation density is increased owing to the decrease in the exciton Bohr radius.

The far-field emission pattern at 10 K after nonresonant cw excitation is shown in Figs. 4(a) and 4(b) for two different δ values. In both cases, the MC is operating in the SCR, as evidenced by the dispersion of the lower emission mode, which we attribute to LPs. Now, the extracted occupancy of the LPB displayed in Fig. 4(c) evidences that when going from slightly positive to very negative δ values, the occupancy of the bottom of the LPB decreases [Fig. 4(c)]. For negative δ values, the energy relaxation of LPs is indeed hindered, due to the more pronounced photon-like character of LPs, and their distribution in k-space is far from thermal equilibrium. This relaxation bottleneck is directly evidenced by the fact that the most salient contribution to the emission arises from high-$\mathbf{k}_\parallel$ states [Fig. 4(a)]: the so-called exciton reservoir.[6] This bottleneck can be overcome either by increasing the carrier density to favor polariton-polariton interactions or by increasing the temperature to favor polariton-phonon interactions or finally by tuning the cavity positively,[10] as the total scattering rate of polaritons scales with the excitonic fraction in their wave function.

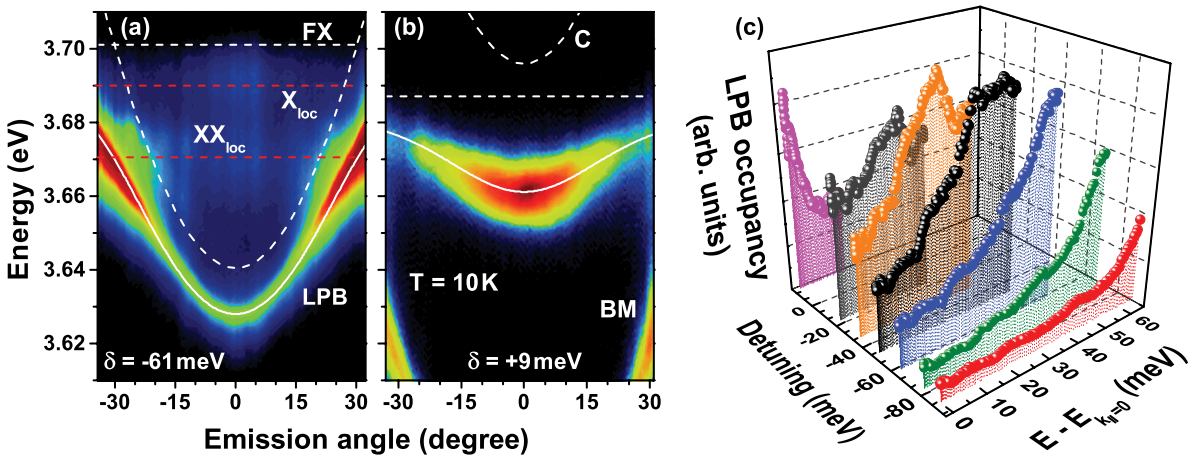

FIG. 4. (Color online) Angle-resolved PL spectra for a detuning (a) $\delta = -61$ meV and (b) $\delta = 9$ meV (arbitrary logarithmic color scale). The spectra have been taken with a cw frequency-doubled Ar^+ laser ($\lambda = 244$ nm) with an excitation power density of 75 W/cm^2. The white solid lines mark the dispersion of the LPB, while the white dashed lines show the uncoupled cavity (C) and FX modes. For negative δ values the localized exciton and biexciton states are well resolved [red (dark gray) dashed lines], whereas for positive δ values a leakage through a Bragg mode (BM) appears. (c) LPB occupancy evolution as a function of δ.

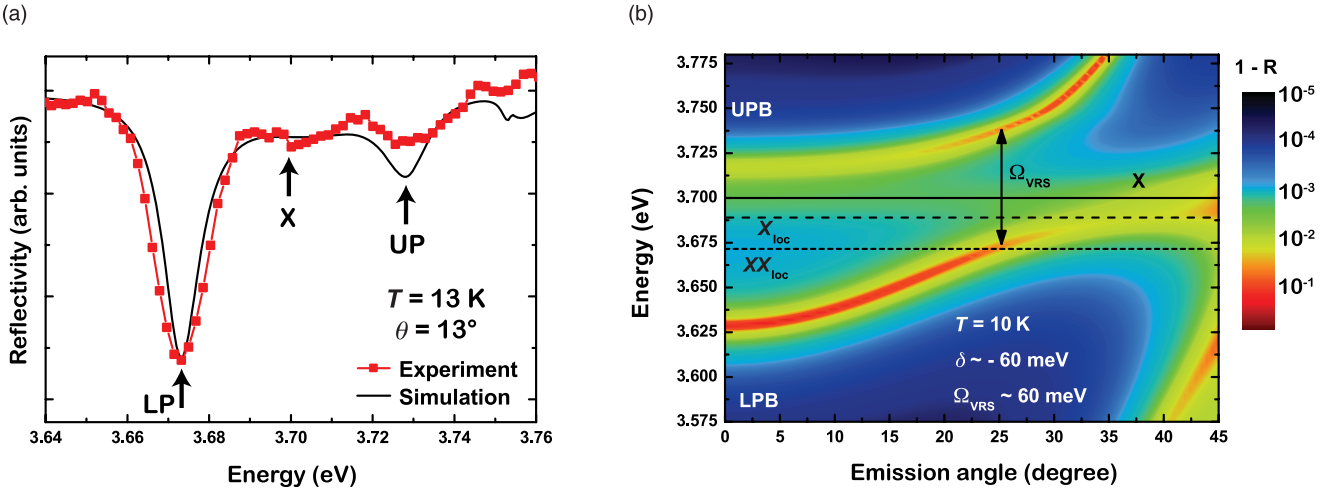

FIG. 5. (Color online) (a) Computed (black solid line) and measured (red symbols) reflectivity spectra of a GaN MQW MC at 13 K taken at an angle of 13°. LP, X, and UP point out the resonances of lower polaritons, free excitons, and upper polaritons, respectively. (b) computed angle resolved reflectivity (R) spectra of a GaN MQW-MC at 10 K for a vacuum Rabi splitting $\Omega_{\mathrm{VRS}} = 60$ meV and a cavity detuning $\delta = -60$ meV. The 67 QW exciton modes have been modeled by 67 independent and inhomogeneously broadened oscillators, giving rise to an optical signature at the energy of the uncoupled exciton. Note that 1−R is displayed in logarithmic scale in order to enhance the visibility of the modes. UPB and LPB denote the UP and LP branches, respectively. Solid, dashed, and short-dash lines show the energy of FXs, localized excitons, and localized biexcitons, respectively.

In the specific case where $\delta = -61$ meV, the LP PL at $\mathbf{k}_{\parallel} = 0$ lies at 3.629 eV at 10 K. From the fitting of the LP PL dispersion considering a vacuum Rabi splitting $\Omega \sim 60$ meV, as determined by previous reflectivity and PL experiments,[15,16] we deduce that the uncoupled exciton and the bottom of the UP branch (UPB) lie at 3.701 and 3.713 eV, respectively [see Fig. 5(b)]. In addition to the PL from LPs, we observe two emission lines at 3.671 and 3.690 eV. These lines are dispersionless and correspond in energy neither to the UPB nor to the uncoupled free QW exciton. The origin of those two modes will be highlighted in the remaining part of this section and the following one, while we describe in Sec. IV C their role in the overall relaxation of LPs in the present MQW MC.

In *real* samples, nonidealities including alloy disorder, QW width fluctuations, or even defects lead to a sharing of the oscillator strength between the polariton modes and the dark excitons.[20] Even if the SCR is preserved, dark excitons may thus exhibit an optical signature in absorption, reflectivity, or PL experiments.[26] On top of this an additional nonideality comes into play for the present structure: QWs located apart from the electric field antinodes are partly uncoupled from the photonic cavity mode and are therefore adding an extra contribution to the optical response. The combination of both effects is responsible for the weak dip observed at the energy of the uncoupled exciton mode in reflectivity measurements [cf. Fig. 5(a)]. This measurement is in agreement with the results of transfer matrix simulations shown in Fig. 5(b).

Similarly to what happens for excitons in the bare active medium sample, uncoupled excitons in the full MC efficiently localize on potential fluctuations distributed along the QW planes. As the MQW and the MC samples have been grown during the same run, the potential fluctuations along the QW planes are likely to be the same in both samples leading us to assume an exciton localization energy of ∼11 meV in both cases.[51] Coming back to the experiments displayed in Fig. 4, where the uncoupled exciton energy lies at 3.701 eV, we deduce that the corresponding emission energy for localized excitons is 3.690 eV: we consequently attribute the nondispersive transition detected at 3.690 eV to the recombination of excitons localized along the QW planes.

B. Cavity biexcitons

In order to reach a deeper understanding of the origin of the 3.671 eV line, we study, hereafter, its emission intensity decay at normal incidence after nonresonant picosecond excitation, together with the one of the localized exciton emission. While the emission from localized excitons decays nonexponentially, the line at 3.671 eV decays exponentially with a decay time $\tau_{XX} = 335$ ps (Fig. 6). After ∼795 ps of decay, we observe that the emission intensity decay of the 3.671 eV line quadratically follows that of excitons. Similarly to the case of the bare-MQW sample [Fig. 2(d)], this characteristic PL decay allows us to attribute the line at 3.671 eV to the radiative dissociation of cavity biexcitons (see Ref. 38 and Appendix). As discussed theoretically in Ref. 20, dark excitons in MQW MCs efficiently bind into biexcitons. These biexcitons then recombine and leave either a dark exciton, a LP or an UP. It is important to notice that for each of these recombination channels, the photon leaving the cavity presents a different energy:

(i) first, a cavity biexciton can dissociate into a photon and a dark exciton. The corresponding biexciton emission energy is then nothing but $\Delta_{XX} = E_X - E_{XX}^B$ for free biexcitons, or $\Delta_{XX} = E_X + E_X^{\mathrm{loc}} - E_{XX}^{\mathrm{loc}} - E_{XX}^B$ when biexcitons are localized. Note that the equality sign might not hold exactly as the MC biexciton binding energy was shown to be slightly modified by the light-matter interaction,[23]

(ii) the radiative dissociation of a cavity biexciton can also directly feed the LPB. Neglecting the dispersion of biexcitons, we get that the biexciton emission energy is

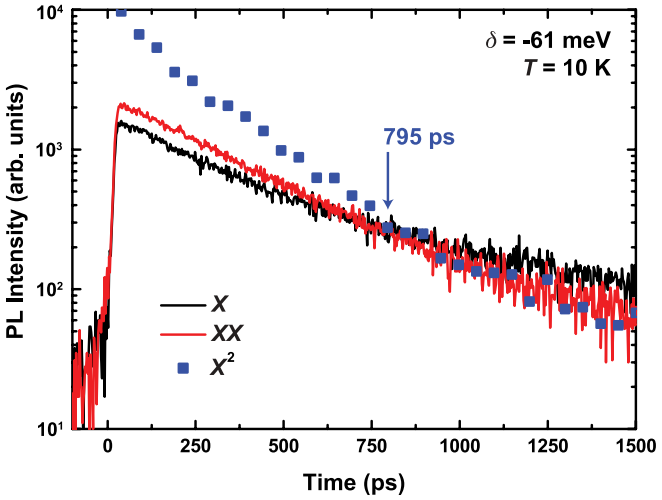

FIG. 6. (Color online) PL decays measured at 10 K for the exciton emission (black) and for the line at 3.671 eV [red (dark gray)], for a cavity detuning of −61 meV. After 795 ps, the time-dependent emission intensity of the line centered at 3.671 eV follows the square of that of the exciton (blue symbols), evidencing its biexcitonic origin.

$\Delta_{XX} = 2E_X - E^B_{XX} - E_{\rm LP}(\mathbf{k}_\parallel^{\rm LP}) > E_X - E^B_{XX}$, where $\mathbf{k}_\parallel^{\rm LP}$ is the in-plane wave vector of the remaining LP,

(iii) finally, the recombination of a biexciton may also leave an UP. Then, the biexciton emission energy is $\Delta_{XX} = 2E_X - E^B_{XX} - E_{\rm UP}(\mathbf{k}_\parallel^{\rm UP}) < E_X - E^B_{XX}$, where $\mathbf{k}_\parallel^{\rm UP}$ is the in-plane wave vector of the remaining UP. We can already note that, in our case, the biexciton emission lies at much too high energy to be ascribed to this recombination channel.

Contrary to excitons, which are dark when their kinetic energy exceeds 0.1 meV,[52,53] biexcitons can couple to light, whatever their in-plane wave vector.[54] This arises from the fact that even if the recombination of a biexciton requires momentum conservation, the remaining wave vector is transferred to the exciton or to the polariton left after the radiative dissociation (Fig. 7). As a consequence, regarding the distributions of excitons and biexcitons in k-space compared to the limited extension of the trap formed by LPs (see Fig. 7), the most probable channels for the recombination of cavity biexcitons are those leaving either an exciton or LP in the reservoir, i.e., at high in-plane momentum beyond the LPB inflection point. It is important to notice here that, as shown by the transfer matrix simulations displayed in Fig. 5(b), 1–R does not strictly go to zero at the emission energy of excitons and biexcitons, meaning that the photons resulting from the recombination of excitons and biexcitons can easily leak out from the cavity. The finite broadening of both the exciton and the cavity modes also increases the density of states available for the radiative dissociation of a given biexciton state, therefore increasing its recombination probability compared to the ideal case treated in Ref. 20. Finally, while uncoupled excitons accumulate, get localized, and then recombine, LPs accumulate in the reservoir. In the low excitation density regime, the latter lose their excess of kinetic energy via interactions with the surrounding electronic population and with acoustic phonons, they relax toward the bottom of the LPB and finally escape from the cavity with a radiative decay time of the order of the picosecond (see Fig. 7 and Ref. 6).

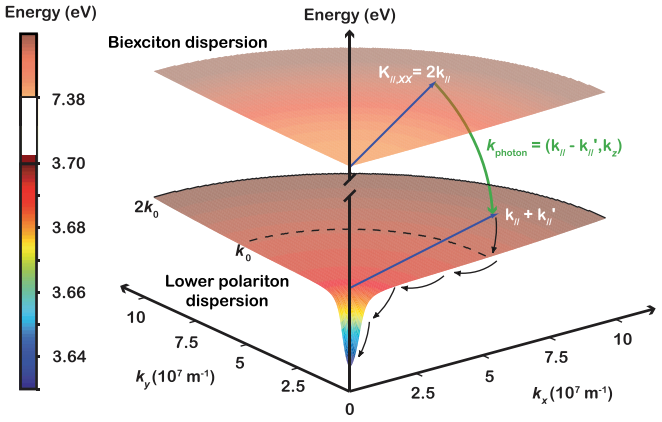

FIG. 7. (Color online) In-plane energy dispersion for LPs and biexcitons in the GaN MQW-MC for a detuning of −61 meV between the cavity and the exciton modes. At negative detuning, the anticrossing behavior between the LP and UP eigenmodes generates a trap for the LPs with very low effective mass at the center of the Brillouin zone. Cavity biexcitons are formed from the binding of two dark excitons. Cavity biexcitons with an in-plane wave vector $\boldsymbol{K}_{\parallel,XX}$ smaller than two times $k_0 = nE_X(0)/\hbar c$ can efficiently couple to the light, where c denotes the speed of light and n is the optical refractive index. When a cavity biexciton recombines [green (medium gray) arrow], a photon and an LP are created, whose wave vectors must verify the conservation of the in-plane momentum. LPs then relax toward the center of the Brillouin zone through the emission of acoustic phonons (dark arrows).

C. Biexciton-assisted polariton relaxation

So far, we have described the available recombination channels for excitons, biexcitons, and polaritons. However, the relative relaxation rates of the different paths available are still unknown. It therefore does not allow us to apprehend which phenomenon is the one limiting the relaxation of polaritons toward the $\mathbf{k}_\parallel = 0$ state and what is the role of the biexcitons in the polariton condensate formation. To solve this issue, we investigate in this section the evolution of the emission intensities and decay times of the different transitions with respect to the cavity detuning, and we finally measure the δ dependence of the polariton lasing threshold. We first display in Fig. 8(a) the evolution of the emission spectra at small angles and after picosecond nonresonant excitation, for cavity detunings ranging from −40 to −160 meV. In addition to the emission from excitons, biexcitons, and LPs, other lines are observed. First, we observe at ∼3.82 eV a broad emission line that we attribute to the $Al_{0.2}Ga_{0.8}N$ barrier [Fig. 8(b)]. We also detect two transitions that fall exactly, independent of the detuning, 91 meV below the exciton and biexciton emission lines. We thus ascribe these two lines to the exciton and cavity biexciton first LO-phonon replica, respectively. Finally, we observe between 3.3 and 3.5 eV several emission lines that, owing to their characteristic energy dispersion, we relate to leakage through Bragg modes.

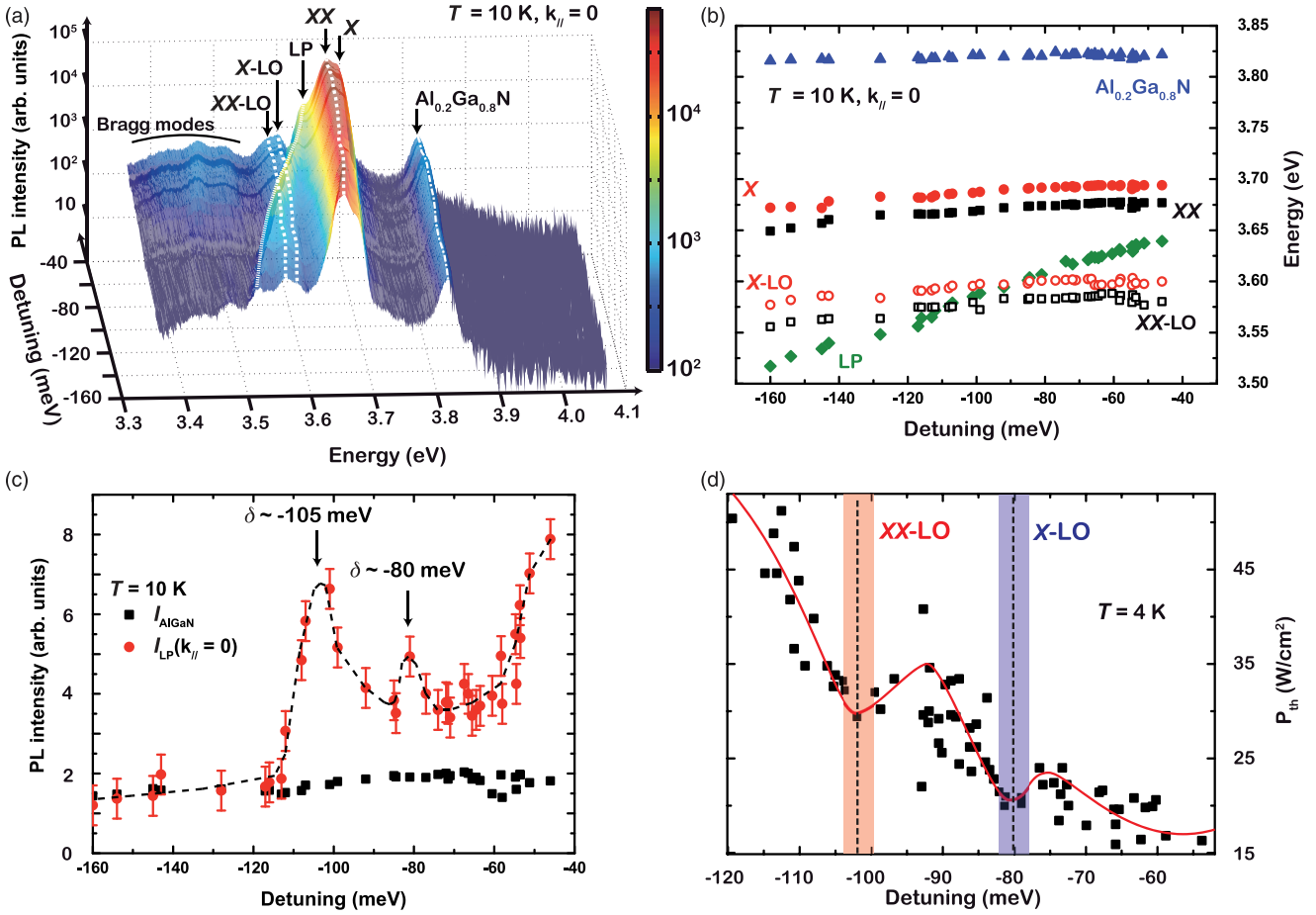

FIG. 8. (Color online) (a) TI PL spectra of the GaN MQW MC taken under nonresonant excitation, at normal incidence at 10 K, with respect to the cavity detuning (δ). White lines are guides to the eye showing the δ dependence of biexciton (XX), exciton, and biexciton first LO-phonon replica (X-LO and XX-LO, respectively), bottom of the LPB (LP) and $Al_{0.2}Ga_{0.8}N$ emission energies. (b) $Al_{0.2}Ga_{0.8}N$, X, XX, LP, X-LO, and XX-LO emission energies with respect to δ. When $\delta = -80$ and -105 meV, LP corresponds in energy to X-LO and XX-LO, respectively. (c) Emission intensity from the (Al,Ga)N (squares) and the bottom of the LPB (circles) measured at 10 K versus δ. The emission intensities from LP and $Al_{0.2}Ga_{0.8}N$ have been obtained after a careful deconvolution of the TI PL spectra displayed in (a). (d) Polariton lasing threshold power density (P_{th}) measured at 4 K under nonresonant pumping with a Nd:YAG laser as a function of δ. Two local minima in P_{th} are observed when $\delta = -80$ and -105 meV. In (c) and (d), lines are guides for the eyes.

When going from a cavity detuning of -40 to -160 meV, keeping the excitation power density constant, we only observe slight variations in the (Al,Ga)N emission intensity, indicating that the injected carrier density has been kept almost constant for all experiments [Fig. 8(c)]. Moreover, although the emission energy of excitons and biexcitons fluctuates when varying δ [the exciton emission energy goes from 3.652 to 3.695 eV, when δ is tuned between -160 and -40 meV, see Fig. 8(b)], due to strain variation along the wedge of the sample, their energy separation is always kept equal to 19 ± 1 meV. We underline also that, for all δ values, the time-decay of the biexciton emission follows quadratically that of the exciton emission after $\sim 700 - 900$ ps (Fig. 9), evidencing that the discussion developed in Secs. III A and III B for $\delta = -61$ meV can be readily extended to the whole range $-40 < \delta < -160$ meV.

Now, in contrast to exciton and biexciton emission lines, the emission intensity from LPs at $\mathbf{k}_{\parallel} = 0$ shows strong variations with respect to δ [Fig. 8(c)]. First, for δ comprised between -40 and -70 meV and for $\delta < -110$ meV, we observe a decrease in the emission intensity of LPs at $\mathbf{k}_{\parallel} = 0$, when δ is reduced. This decrease in emission intensity at normal incidence for LPs arises from the fact that, when going from slightly to very negative detunings, the scattering rate of LPs with acoustic phonons decreases owing to the increasing photonic character of the polaritons, hampering the polariton relaxation toward the Brillouin zone center.[6] Polaritons in the reservoir are therefore more likely to escape from the cavity through leaky modes (or to recombine nonradiatively) than to relax down to the bottom of the branch. Superimposed to this general trend, two local maxima for the emission intensity of LPs at $\mathbf{k}_{\parallel} = 0$ are observed. The first one occurs when $\delta = -80$ meV, i.e., when the energy of LP($\mathbf{k}_{\parallel} = 0$) corresponds to that of the first LO-phonon replica of the exciton. This behavior is similar to that first reported by Boeuf *et al.* for CdTe MCs, where a local minimum in the polariton lasing threshold was observed, when the energy difference between the bottom of the LPB and the excitonic reservoir matches the energy of

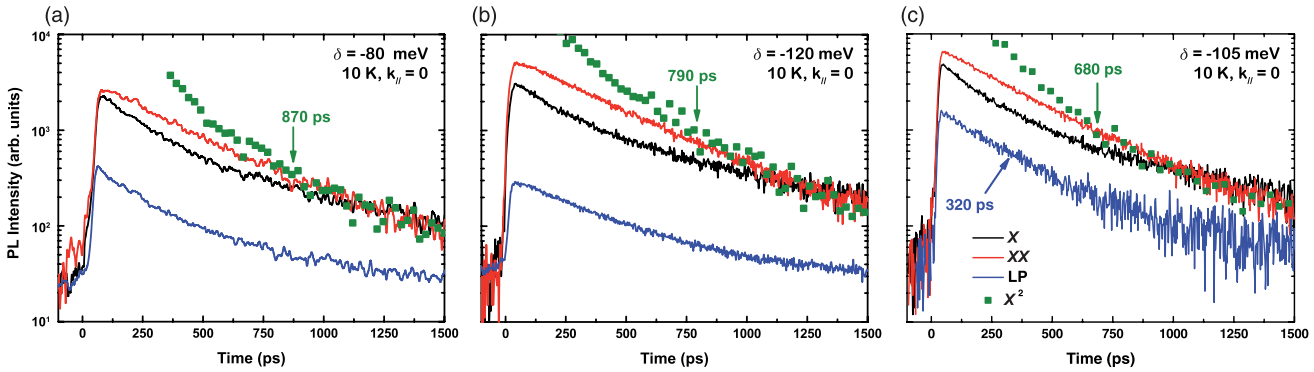

FIG. 9. (Color online) Low-temperature PL decays for the exciton (black), biexciton [red (dark gray)], and LP [blue (medium gray)] emissions at $\mathbf{k}_{\parallel} = 0$, for a detuning $\delta = -80$ (a), -120 (b), and -105 meV (c). In (a) and (b), the LP emission follows the same dynamics as the exciton. On the contrary, when $\delta = -105$ meV (c), both the biexciton and the LP emissions exponentially decay with a decay time of 320 ps. For all detunings, the biexciton emission intensity follows the square of that of the exciton (green symbols) after ~700–900 ps, evidencing full thermalization between exciton and biexciton states.

one LO-phonon.[55] In our case, the local increase in the PL intensity of LP($\mathbf{k}_{\parallel} = 0$) evidences the efficient LO-phonon assisted transfer of both uncoupled excitons and high-$\mathbf{k}_{\parallel}$ LPs to the bottom of the LPB. A second local maximum is observed for $\delta \sim -105$ meV, when the bottom of the LPB corresponds in energy to that of the first LO-phonon replica *of the biexciton*. In the same way, we attribute this observation to the direct feeding of $\mathbf{k}_{\parallel} = 0$ LP states by the radiative dissociation of cavity biexcitons assisted by one LO-phonon. In other words, the processes "$XX \rightarrow \mathrm{LP}(\mathbf{k}_{\parallel} = 0) + \mathrm{LO} + X$" and "$XX \rightarrow \mathrm{LP}(\mathbf{k}_{\parallel} = 0) + \mathrm{LO} + \mathrm{LP}(\text{high-}\mathbf{k}_{\parallel})$" provide efficient ways of relaxation toward the bottom of the LPB. If we now monitor the evolution with δ of the polariton condensation threshold under nonresonant optical pumping at 4 K, we observe two minima for $\delta = -80$ and -105 meV [Fig. 8(d)]. Similarly to Refs. 55–57, we attribute the former minimum to the relaxation of exciton in the reservoir by the emission of one LO-phonon, allowing for bypassing the relaxation bottleneck. Regarding the second minimum polariton lasing threshold lying at $\delta = -105$ meV, it corresponds to the case where LP($\mathbf{k}_{\parallel} = 0$) arise from the LO-phonon-assisted radiative dissociation of cavity biexcitons.

To further support our view, we display in Fig. 9 the decay of the luminescence from LP($\mathbf{k}_{\parallel} = 0$) for various δ values. For δ comprised between -40 and -95 meV and between -110 and -160 meV, we observe that the LP PL at normal incidence decays nonexponentially and follows at all times the same dynamics as the exciton PL [Figs. 9(a) and 9(b)]. This behavior demonstrates (i) that the uncoupled exciton branches are at thermal equilibrium with the LP reservoir and (ii) that the decay of the reservoir itself is limited by LP-LP and LP-acoustic phonons scattering. In other words, the PL decay of the bottom of the LPB is imposed by the relaxation of LPs from the reservoir to the trap.[58] Of course, in the specific case where $\delta = -80$ meV, and in agreement with the previous discussion, the relaxation of excitons and LPs in the reservoir is dominated by their scattering with LO-phonons rather than with acoustic phonons. On the contrary, when $\delta \sim -105$ meV, LPs at $\mathbf{k}_{\parallel} = 0$ and biexcitons both decay exponentially with a decay time of 320 ps [Fig. 9(c)]. In the latter situation, and in agreement with the data displayed in Figs. 8(c) and 8(d), the feeding of the $\mathbf{k}_{\parallel} = 0$ LPs states is then dominated by the radiative dissociation of cavity biexcitons.

A deeper understanding of the role played by biexcitons in semiconductor MCs operating in the SCR is of special interest as they strongly interact with the polariton population. Under coherent (resonant) excitation, the presence of biexcitons can significantly alter the light-matter coupling. As already mentioned, with increasing pump intensity, a progressive transfer of oscillator strength from the exciton to the biexciton transition was evidenced by pump-probe experiments, favoring the formation of biexciton polaritons to the detriment of exciton polaritons.[24] More recently, the progressive formation of biexcitons from two excitons of opposite spins has been shown to hinder the light-matter coupling through the introduction of nonlinear losses, favoring a given spin population at the expense of the other one.[59] Biexcitons should be thus included in the description of the relaxation in QW-based MCs in order to complete the picture of the interactions occurring within the polariton ensemble. This particularly affects the renormalization of the polariton dispersion. In the usual framework, only polariton-exciton and polariton-polariton interactions are considered resulting in a linear scaling of the polariton ground-state energy with its population—below and above the condensation threshold. This behavior is described by the two interaction constants: $\alpha_1 > 0$, describing the repulsive interaction between polaritons with the same spin and $\alpha_2 < 0$, the attractive interaction between polaritons with opposite spin.[60] It is generally assumed that $|\alpha_2| \ll \alpha_1$, due to the dominating contribution of the exchange interaction term in two-dimensional systems.[61] It was shown that the biexciton-mediated interaction results in an effective polariton-polariton attraction that strongly affects the sign and strength of α_2[62,63] and can increase the efficiency of the LP-LP scattering processes due to the appearance of the singlet biexciton state as an intermediate transition.[64] Interestingly, depending on the detuning, the ratio α_2/α_1 can eventually go below -1, i.e., the attraction overcomes the repulsion, making possible the coexistence of condensation in real and reciprocal spaces.[63] We believe that, thanks to the large biexciton binding energy in GaN QWs, III-nitride based MCs are prototypical systems to gain a deeper understanding

of the biexciton contribution to the α_1 and α_2 coefficients. This will not only allow for a better comprehension of the polariton branch renormalization and the overall relaxation dynamics, but this can also offer a better tuning of polariton spin-dependent devices such as ultrafast optical spin switches.[65]

V. CONCLUSION

In summary, the radiative dissociation of biexcitons in a MQW III-nitride based MC operating in the SCR has been investigated by means of continuous wave and TR PL techniques. The direct observation of cavity biexciton emission has been facilitated by the nonidealities of the cavity active medium, which lead to a redistribution of the oscillator strength between the polariton states and the dark QW excitons. When the energy of the bottom of the LPB corresponds to that of the first LO-phonon replica of the cavity biexciton, we observe an enhanced scattering of polaritons toward the $\mathbf{k}_{\parallel} = 0$ state, as well as a decrease in condensation threshold. This fact, combined with the observation of identical decay rates, evidences that, for this peculiar detuning, the mechanism limiting the energy relaxation of polaritons is the dissociation of cavity biexcitons into a LP, a LO phonon, and an exciton, rather than the inelastic scattering of exciton-polaritons with acoustic phonons. Our study clearly evidences that biexcitons have to be taken into account when describing the polariton relaxation in MCs, and we believe that it will stimulate more work aiming at understanding the role of multiexcitonic complexes on the formation of polariton condensates.

ACKNOWLEDGMENTS

The authors would like to thank R. Rochat, N. Leiser, D. Trolliet, and N. Trolliet for technical support. We acknowledge the financial support from the NCCR Quantum Photonics, research instrument of the Swiss National Science Foundation through Grant No. 129715 and Grant No. 200020-113542, and from the EU-project Clermont4 (Grant No. FP7-235114).

APPENDIX

We detail here the relations describing the equilibrium between free and localized excitons and biexcitons in order to show that in a thermalized system, the time dependence of localized biexciton emission follows the square of the time dependence of the localized exciton emission. For completeness, we also account in our modeling for free electron-hole pairs.

Using the expression given in Refs. 66 and 67, the thermal dissociation of free QW excitons into free electron-hole pairs writes:

$$\frac{N_e N_h}{N_X^{fr}} = \frac{\mu kT}{2\pi\hbar^2} \exp\left[-\frac{E_X^B}{kT}\right], \tag{A1}$$

where N_e, N_h, and N_X^{fr} are the densities of electrons, holes, and FXs confined in the QW, respectively, and μ is the exciton-reduced mass. Similarly, Saha's law for FXs and biexcitons is given by:

$$\frac{\left(N_X^{fr}\right)^2}{N_{XX}^{fr}} = \frac{MkT}{\pi\hbar^2} \exp\left[-\frac{E_{XX}^B}{kT}\right], \tag{A2}$$

where N_{XX}^{fr} is the biexciton density and M is the exciton translational mass. In presence of disorder, QW excitons localize due to interface roughness, and the thermal exchange between localized and free QW excitons is described by:[68]

$$\frac{N_X^{fr}}{N_X^{\mathrm{loc}}} = \frac{2MkT}{\pi\hbar^2 N_D} \exp\left[-\frac{E_X^{\mathrm{loc}}}{kT}\right], \tag{A3}$$

where N_X^{loc} is the density of localized excitons and N_D is the density of localizing centers. As shown in the present paper, biexcitons also efficiently localize along the QW plane. We therefore readily extend Eq. (A3) to the equilibrium between

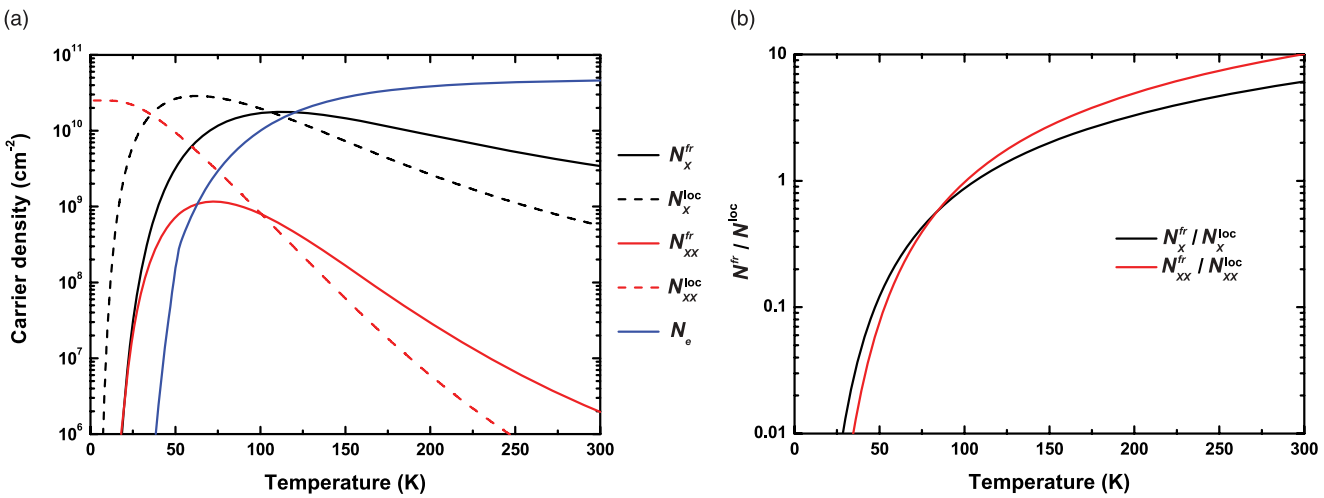

FIG. 10. (Color online) (a) Calculated-free (solid lines) and localized (dashed lines) densities of excitons, biexcitons, and electrons [black, red (dark gray), and blue (medium gray), respectively] confined in a 1.2-nm-thick $Al_{0.2}Ga_{0.8}N/GaN$ QW for a photogenerated pair density of 5×10^{10} cm^{-2}. (b) Ratios between free and localized exciton (black) and biexciton [red (dark gray)] densities with respect to temperature. At 200 K, excitons and biexcitons are mainly delocalized along the QW plane.

localized and free biexcitons, yielding:

$$\frac{N_{XX}^{fr}}{N_{XX}^{\mathrm{loc}}} = \frac{4MkT}{\pi\hbar^2 N_D}\exp\left[-\frac{E_{XX}^{\mathrm{loc}}}{kT}\right], \tag{A4}$$

where N_{XX}^{loc} is the density of localized biexcitons. In Eqs. (A3) and (A4), we have assumed that the same density of localizing centers was accessible for both excitons and biexcitons. Combining Eqs. (A2)–(A4) then leads to:

$$\frac{\left(N_X^{\mathrm{loc}}\right)^2}{N_{XX}^{\mathrm{loc}}} = N_D \exp\left[-\frac{E_{XX}^B + E_{XX}^{\mathrm{loc}} - 2E_X^{\mathrm{loc}}}{kT}\right]. \tag{A5}$$

The emission intensity for a distribution of excitons is proportional to the radiative part of its temporal derivative. Therefore, in a thermalized system, the time-dependent emission intensity from localized biexcitons $I_{XX}^{\mathrm{loc}}(t)$ follows at all times the square of that of localized excitons $I_X^{\mathrm{loc}}(t)$. Following the procedure described in Ref. 69, we can numerically calculate for all temperatures the densities of excitons, biexcitons, and free carriers confined in the QWs. In these calculations, we have taken $E_X^B = 43$ meV (Fig. 1), $E_X^{\mathrm{loc}} = 11$ meV (Fig. 2), and $E_{XX}^B = 22$ meV and $E_{XX}^{\mathrm{loc}} = 16$ meV (Fig. 3), and we have tentatively assumed that $N_D = 3 \times 10^{12}$ cm^{-2}, as determined previously in Ref. 53. In addition, as our layers are nominally undoped, we take $N_e = N_h$. The result of our calculations, displayed in Fig. 10 for a photogenerated carrier density $N_{\mathrm{tot}} = 5 \times 10^{10}$ cm^{-2}, verifies *a posteriori* that at 200 K, excitons and biexcitons are mostly delocalized.

*Corresponding author: pmc53@cam.ac.uk

†Present address: Cavendish Laboratory, University of Cambridge, J. J. Thomson Avenue, Cambridge CB3 0HE, United Kingdom.

[1] C. Weisbuch, M. Nishioka, A. Ishikawa, and Y. Arakawa, Phys. Rev. Lett. **69**, 3314 (1992).

[2] P. G. Savvidis, J. J. Baumberg, R. M. Stevenson, M. S. Skolnick, D. M. Whittaker, and J. S. Roberts, Phys. Rev. Lett. **84**, 1547 (2000).

[3] J. Kasprzak, M. Richard, S. Kundermann, A. Baas, P. Jeambrun, J. M. J. Keeling, F. M. Marchetti, M. H. Szymanska, R. André, J. L. Staehli, V. Savona, P. B. Littlewood, B. Deveaud, and Le Si Dang, Nature (London) **443**, 409 (2006).

[4] S. Christopoulos, G. Baldassari Höger von Högersthal, A. J. D. Grundy, P. G. Lagoudakis, A. V. Kavokin, J. J. Baumberg, G. Christmann, R. Butté, E. Feltin, J.-F. Carlin, and N. Grandjean, Phys. Rev. Lett. **98**, 126405 (2007).

[5] A. Imamoglu, R. J. Ram, S. Pau, and Y. Yamamoto, Phys. Rev. A **53**, 4250 (1996).

[6] F. Tassone, C. Piermarocchi, V. Savona, A. Quattropani, and P. Schwendimann, Phys. Rev. B **56**, 7554 (1997).

[7] C. Ciuti, P. Schwendimann, B. Deveaud, and A. Quattropani, Phys. Rev. B **62**, R4825 (2000).

[8] Y. G. Rubo, G. Malpuech, A. V. Kavokin, and P. Bigenwald, Phys. Rev. Lett. **91**, 156403 (2003).

[9] R. Butté, G. Delalleau, A. I. Tartakovskii, M. S. Skolnick, V. N. Astratov, J. J. Baumberg, G. Malpuech, A. Di Carlo, A. V. Kavokin, and J. S. Roberts, Phys. Rev. B **65**, 205310 (2002).

[10] A. I. Tartakovskii, M. Emam-Ismail, R. M. Stevenson, M. S. Skolnick, V. N. Astratov, D. M. Whittaker, J. J. Baumberg, and J. S. Roberts, Phys. Rev. B **62**, R2283 (2000).

[11] J. Bloch, T. Freixanet, J.-Y. Marzin, V. Thierry-Mieg, and R. Planel, Appl. Phys. Lett. **73**, 1694 (1998).

[12] G. Malpuech, A. Kavokin, A. Di Carlo, and J. J. Baumberg, Phys. Rev. B **65**, 153310 (2002).

[13] E. Wertz, L. Ferrier, D. D. Solnyshkov, P. Senellart, D. Bajoni, A. Miard, A. Lemaître, G. Malpuech, and J. Bloch, Appl. Phys. Lett. **95**, 051108 (2009).

[14] J. Levrat, R. Butté, E. Feltin, J.-F. Carlin, N. Grandjean, D. Solnyshkov, and G. Malpuech, Phys. Rev. B **81**, 125305 (2010).

[15] G. Christmann, R. Butté, E. Feltin, A. Mouti, P. A. Stadelmann, A. Castiglia, J.-F. Carlin, and N. Grandjean, Phys. Rev. B **77**, 085310 (2008).

[16] G. Christmann, R. Butté, E. Feltin, J.-F. Carlin, and N. Grandjean, Appl. Phys. Lett. **93**, 051102 (2008).

[17] R. Butté, J. Levrat, G. Christmann, E. Feltin, J.-F. Carlin, and N. Grandjean, Phys. Rev. B **80**, 233301 (2009).

[18] D. M. Whittaker, P. Kinsler, T. A. Fisher, M. S. Skolnick, A. Armitage, A. M. Afshar, M. D. Sturge, and J. S. Roberts, Phys. Rev. Lett. **77**, 4792 (1996).

[19] V. Savona, C. Piermarocchi, A. Quattropani, F. Tassone, and P. Schwendimann, Phys. Rev. Lett. **78**, 4470 (1997).

[20] G. C. La Rocca, F. Bassani, and V. M. Agranovich, J. Opt. Soc. Am. B **15**, 652 (1998).

[21] M. Kuwata-Gonokami, S. Inouye, H. Suzuura, M. Shirane, R. Shimano, T. Someya, and H. Sakaki, Phys. Rev. Lett. **79**, 1341 (1997).

[22] X. Fan, H. Wang, H. Q. Hou, and B. E. Hammons, Phys. Rev. B **57**, R9451 (1998).

[23] P. Borri, W. Langbein, U. Woggon, A. Esser, J. R. Jensen, and J. M. Hvam, Semicond. Sci. Technol. **18**, S351 (2003).

[24] M. Saba, F. Quochi, C. Ciuti, U. Oesterle, J. L. Staehli, B. Deveaud, G. Bongiovanni, and A. Mura, Phys. Rev. Lett. **85**, 385 (2000).

[25] G. Christmann, D. Simeonov, R. Butté, E. Feltin, J.-F. Carlin, and N. Grandjean, Appl. Phys. Lett. **89**, 261101 (2006).

[26] R. Houdré, R. P. Stanley, and M. Ilegems, Phys. Rev. A **53**, 2711 (1996).

[27] F. Stokker-Cheregi, A. Vinattieri, E. Feltin, D. Simeonov, J.-F. Carlin, R. Butté, N. Grandjean, and M. Gurioli, Phys. Rev. B **77**, 125342 (2008).

[28] K. Okada, Y. Yamada, T. Taguchi, F. Sasaki, S. Kobayashi, T. Tani, S. Nakamura, and G.-I. Shinomiya, Jpn. J. Appl. Phys. **35**, L787 (1996).

[29] Y. Kawakami, Z. G. Peng, Y. Narukawa, S. Fujita, and S. Nakamura, Appl. Phys. Lett. **69**, 1414 (1996).

[30] S. Amloy, K. H. Yu, K. F. Karlsson, R. Farivar, T. G. Andersson, and P. O. Holtz, Appl. Phys. Lett. **99**, 251903 (2011).

[31] E. Feltin, D. Simeonov, J.-F. Carlin, R. Butté, and N. Grandjean, Appl. Phys. Lett. **90**, 021905 (2007).

[32] M. Leroux, N. Grandjean, J. Massies, B. Gil, P. Lefebvre, and P. Bigenwald, Phys. Rev. B **60**, 1496 (1999).

[33] J.-W. Wu, Solid State Commun. **67**, 911 (1988).

[34] R. Zimmermann and D. Bimberg, Phys. Rev. B **47**, 15789 (1993).

[35] A. Bellabchara, P. Lefebvre, P. Christol and H. Mathieu, Phys. Rev. B **50**, 11840 (1994).
[36] G. Bastard, E. E. Mendez, L. L. Chang, and L. Esaki, Phys. Rev. B **26**, 1974 (1982).
[37] P. Lefebvre, S. Kalliakos, T. Bretagnon, P. Valvin, T. Taliercio, B. Gil, N. Grandjean, and J. Massies, Phys. Rev. B **69**, 035307 (2004).
[38] J. C. Kim, D. R. Wake, and J. P. Wolfe, Phys. Rev. B **50**, 15099 (1994).
[39] C. Weisbuch, R. Dingle, A. C. Gossard, and W. Wiegmann, Solid State Commun. **38**, 709 (1981).
[40] F. Natali, Y. Cordier, J. Massies, S. Vezian, B. Damilano, and M. Leroux, Phys. Rev. B **79**, 035328 (2009).
[41] Note that this value is higher than what was reported in the literature for (Al,Ga)N layers with similar Al-content, see, for instance, K. B. Lee, P. J. Parbrook, T. Wang, F. Ranalli, T. Martin, R. S. Balmer, and D. J. Wallis, J. Appl. Phys. **101**, 053513 (2007).
[42] W. Langbein and J. M. Hvam, Phys. Rev. B **59**, 15405 (1999).
[43] Y. Yamada, Y. Ueki, K. Nakamura, T. Taguchi, A. Ishibashi, Y. Kawaguchi, and T. Yokogawa, Phys. Rev. B **70**, 195210 (2004).
[44] S. T. Cundiff, T. Zhang, A. D. Bristow, D. Karaiskaj, and X. Dai, Acc. Chem. Res. **42**, 1423 (2009).
[45] D. Birkedal, J. Singh, V. G. Lyssenko, J. Erland, and J. M. Hvam, Phys. Rev. Lett. **76**, 672 (1996).
[46] B. Deveaud, T. C. Damen, J. Shah, and C. W. Tu, Appl. Phys. Lett. **51**, 828 (1987).
[47] Below the condensation threshold, J = 2 excitons create a reservoir of dark excitons and dark biexcitons, which leads to an increase in radiative lifetime for both the exciton and biexciton populations. Above the condensation threshold, the presence of this dark reservoir slightly increases the energy of the polariton condensate, therefore contributing to the α_2 term discussed at the end of the paper.
[48] N. Grandjean, B. Damilano, S. Dalmasso, M. Leroux, M. Laügt, and J. Massies, J. Appl. Phys. **86**, 3714 (1999).
[49] V. Savona, L. C. Andreani, P. Schwendimann, and A. Quattropani, Solid State Commun. **93**, 733 (1995).
[50] D. Solnyshkov, H. Ouerdane, and G. Malpuech, J. Appl. Phys. **103**, 016101 (2008).
[51] Note that despite the present inhomogeneous broadening of 11 meV, the strong coupling regime is preserved as we measure a Rabi splitting of 60 meV.
[52] L. C. Andreani, F. Tassone, and F. Bassani, Solid State Commun. **77**, 641 (1991).
[53] P. Corfdir, J. Levrat, A. Dussaigne, P. Lefebvre, H. Teisseyre, I. Grzegory, T. Suski, J.-D. Ganière, N. Grandjean, and B. Deveaud-Plédran, Phys. Rev. B **83**, 245326 (2011).
[54] D. S. Citrin, Phys. Rev. B **50**, 17655 (1994).
[55] F. Boeuf, R. André, R. Romestain, Le Si Dang, E. Péronne, J.-F. Lampin, D. Hulin, and A. Alexandrou, Phys. Rev. B **62**, R2279 (2000).
[56] M. Maragkou, A. J. D. Grundy, T. Ostatnicky, and P. G. Lagoudakis, Appl. Phys. Lett. **97**, 111110 (2010).
[57] L. Orosz, F. Réveret, F. Médart, P. Disseix, J. Leymarie, M. Mihailovic, D. Solnyshkov, G. Malpuech, J. Zuniga-Pérez, F. Semond, M. Leroux, S. Bouchoule, X. Lafosse, M. Mexis, C. Brimont, and T. Guillet, Phys. Rev. B **85**, 121201(R) (2012).
[58] B. Sermage, S. Long, I. Abram, J. Y. Marzin, J. Bloch, R. Planel, and V. Thierry-Mieg, Phys. Rev. B **53**, 16516 (1996).
[59] T. K. Paraiso, M. Wouters, Y. Léger, F. Morier-Genoud, and B. Deveaud-Plédran, Nat. Mater. **9**, 655 (2010).
[60] Y. G. Rubo, A. V. Kavokin, and I. A. Shelykh, Phys. Lett. A **358**, 227 (2007).
[61] C. Ciuti, V. Savona, C. Piermarocchi, A. Quattropani, and P. Schwendimann, Phys. Rev. B **58**, 7926 (1998).
[62] M. Wouters, Phys. Rev. B **76**, 045319 (2007).
[63] M. Vladimirova, S. Cronenberger, D. Scalbert, K. V. Kavokin, A. Miard, A. Lemaître, J. Bloch, D. Solnyshkov, G. Malpuech, and A. V. Kavokin, Phys. Rev. B **82**, 075301 (2010).
[64] A. I. Tartakovskii, D. N. Krizhanovskii, and V. D. Kulakovskii, Phys. Rev. B **62**, R13298 (2000).
[65] R. Cerna, Ph.D. thesis, Thèse n° 5014, Ecole Polytechnique Fédérale de Lausanne, Switzerland, 2011; R. Cerna, T. K. Paraïso, Y. Léger, M. Wouters, F. Morier-Genoud, M. T. Portella-Oberli, and B. Deveaud-Plédran, presented at the 11th International Conference on Physics of Light-Matter Coupling in Nanostructures, Berlin (2011) (unpublished).
[66] D. S. Chemla, D. A. B. Miller, P. W. Smith, A. C. Gossard, and W. Wiegmann, IEEE J. Quantum Electron. **20**, 265 (1984).
[67] We use an expression similar to the one for the dissociation of excitons in free electron-hole pairs, see M. Colocci, M. Gurioli, and A. Vinattieri, J. Appl. Phys. **68**, 2809 (1990).
[68] D. S. Citrin, Phys. Rev. B **47**, 3832 (1993).
[69] P. Corfdir, A. Dussaigne, H. Teisseyre, T. Suski, I. Grzegory, P. Lefebvre, E. Giraud, J.-D. Ganière, N. Grandjean, and B. Deveaud-Plédran, J. Appl. Phys. **111**, 033517 (2012).